

The Combined Influence of Lower Band Chorus and ULF waves on Radiation Belt Electron Fluxes at Individual L-shells

Laura E. Simms¹, Mark J. Engebretson¹, Craig J. Rodger², Stavros Dimitrakoudis³, Ian Mann³, and Peter J Chi⁴

¹Department of Physics, Augsburg University

²University of Otago

³University of Alberta

⁴University of California Los Angeles

November 21, 2022

Abstract

We investigate the timing and relative influence of VLF in the chorus frequency range observed by the DEMETER spacecraft and ULF wave activity from ground stations on daily changes in electron flux (0.23 to over 2.9 MeV) observed by the HEO-3 spacecraft. At each L shell, we use multiple regression to investigate the effects of each wave type and each daily lag independent of the others. We find that reduction and enhancement of electrons occur at different time scales. Chorus power spectral density and ULF wave power are associated with immediate electron decreases on the same day but with flux enhancement 1-2 days later. ULF is nearly always more influential than chorus on both increases and decreases of flux, although chorus is often a significant factor. There was virtually no difference in correlations of ULF Pc3, Pc4, or Pc5 with electron flux. A synergistic interaction between chorus and ULF waves means that enhancement is most effective when both waves are present, pointing to a two-step process where local acceleration by chorus waves first energizes electrons which are then brought to even higher energies by inward radial diffusion due to ULF waves. However, decreases in flux due to these waves act additively. Chorus and ULF waves combined are most effective at describing changes in electron flux at >1.5 MeV. At lower L (2-3), correlations between ULF and VLF (likely hiss) with electron flux were low. The most successful models, over L=4-6, explained up to 47.1% of the variation in the data.

1
2
3
4
5
6
7
8
9
10
11
12
13
14
15
16
17
18
19
20
21
22
23
24
25

The Combined Influence of Lower Band Chorus and ULF waves on Radiation Belt Electron Fluxes at Individual L-shells

Laura E. Simms¹, Mark J. Engebretson¹, Craig J. Rodger², Stavros Dimitrakoudis³, I.R. Mann³, and Peter J. Chi⁴

¹ Augsburg University, Minneapolis, MN, USA

² University of Otago, Dunedin, New Zealand

³ University of Alberta, Edmonton, Canada

⁴ UCLA, Los Angeles, CA, USA

Corresponding author: Laura E. Simms (*simmsl@augsborg.edu*)

Key Points:

- VLF and ULF waves are associated with same day electron (>1.5 MeV) decreases but with flux enhancement 1-2 days later.
- ULF is nearly always more influential than chorus, but electron enhancement is most effective when both wave types are present.
- Both VLF and ULF are more influential at L 4-6 than at lower altitudes.

26 Abstract

27 We investigate the timing and relative influence of VLF in the chorus frequency range observed by the
28 DEMETER spacecraft and ULF wave activity from ground stations on daily changes in electron flux (0.23
29 to over 2.9 MeV) observed by the HEO-3 spacecraft. At each L shell, we use multiple regression to
30 investigate the effects of each wave type and each daily lag independent of the others. We find that
31 reduction and enhancement of electrons occur at different time scales. Chorus power spectral density
32 and ULF wave power are associated with immediate electron decreases on the same day but with flux
33 enhancement 1-2 days later. ULF is nearly always more influential than chorus on both increases and
34 decreases of flux, although chorus is often a significant factor. There was virtually no difference in
35 correlations of ULF Pc3, Pc4, or Pc5 with electron flux. A synergistic interaction between chorus and ULF
36 waves means that enhancement is most effective when both waves are present, pointing to a two-step
37 process where local acceleration by chorus waves first energizes electrons which are then brought to
38 even higher energies by inward radial diffusion due to ULF waves. However, decreases in flux due to
39 these waves act additively. Chorus and ULF waves combined are most effective at describing changes in
40 electron flux at >1.5 MeV. At lower L (2-3), correlations between ULF and VLF (likely hiss) with electron
41 flux were low. The most successful models, over $L=4-6$, explained up to 47.1% of the variation in the
42 data.

43

44

45

46 1. Introduction

47

48 Both chorus and ULF Pc5 waves are thought to influence electron flux levels, increasing them in some
49 situations and decreasing them in others. Observations of single storms show that interactions with
50 chorus can scatter electrons into the loss cone (Clilverd et al., 2016; Horne and Thorne, 2003; Shprits et
51 al., 2007, 2008; Thorne et al., 2005) while ULF Pc5 waves can lead to loss through a combination of
52 outward radial diffusion and magnetopause shadowing (Katsavrias et al., 2015; Kellerman and Shprits,
53 2012; Loto'aniu et al., 2010; Mann et al., 2012; Ozeke et al., 2020; Turner et al., 2012). However,
54 chorus may also result in flux enhancement through local acceleration (Horne et al., 2005; Katsavrias et
55 al., 2015; Reeves, 2013; Shprits et al., 2008; Summers et al., 1998), while ULF Pc5 waves accelerate
56 electrons through inward radial diffusion (e.g., Hao et al., 2019; Katsavrias et al., 2019; Mann et al.,
57 2004) and direct interaction (Claudepierre et al., 2013; Hao et al., 2014; Zong et al., 2009; Zong et al.,
58 2017).

59

60 Both wave types often occur simultaneously before or during changes in electron flux levels (Li et al.,
61 2005). It requires further investigation to determine whether they contribute equally to electron flux
62 levels. Katsavrias et al. (2015) found that over $L=3-5$, the electron population above 300 MeV/G
63 increased when both chorus (inferred from the ratio of precipitating to trapped electron fluxes using
64 POES data in low Earth orbit) and ULF wave power were high, but depleted when only ULF wave activity
65 was high. They interpreted this to mean that chorus was the dominant driver of electron acceleration,
66 but ULF waves, via outward diffusion, resulted in depletion. In a different pair of storms, inferred chorus
67 appeared to accelerate electrons to relativistic energies while ULF waves further accelerated this

68 population to ultrarelativistic energies through inward radial diffusion (Katsavrias et al., 2019). Using
69 results from superposed epoch analysis, flux enhancements were associated with VLF activity (inferred
70 from microbursts) around $L=4.5$, but at L shells above that, the flux association was stronger with ULF
71 activity (O'Brien et al., 2003). Analyzing effects simultaneously using multiple regression, ULF wave
72 power at geosynchronous orbit was found to be of somewhat more influence on electron flux levels
73 (>1.5 MeV) than satellite-observed chorus power spectral density (Simms et al., 2018ab).

74
75 There is, however, still a need to investigate these simultaneous wave effects by L shell, over multiple
76 days, using analyses which study the effect of each factor independent of the others. We use partial
77 correlation analysis to study the influence of each wave type over several days. From these analyses, we
78 are able to determine both when the waves are most influential, and to separate the positive and
79 negative effects that occur on different days. Using multiple regression, we study the separate effects
80 of each wave type on each day. We also explore the nonlinear action of waves on electron flux by
81 including quadratic terms, and whether ULF and VLF waves act both additively and synergistically by
82 including a multiplicative term (Neter et al., 1985).

83
84 In this study, we use electron flux data (HEO-3 satellite) gathered at each L shell ($L=1.75-9$). We use
85 satellite-observed VLF power spectral density (PSD) in the lower band chorus range from the DEMETER
86 satellite, binned by L -shell over $L=1.75-6$. These waves are assumed to be predominately chorus above
87 $L=3$ and predominately hiss below this (Bortnik et al., 2008; Carpenter and Park, 1973). This differs from
88 previous studies of VLF correlation by L shell with electron flux as the VLF measure is neither a proxy
89 from microburst observation nor ground-based VLF data which does not as accurately reflect VLF wave
90 activity occurring in space (Simms et al., 2019). We compare the effects of ULF Pc3, Pc4, and Pc5 data
91 from ground-based stations, Pc5 from $L>3$.

92
93

94

95

96 2. Data

97 Data covered the time period 11 Aug 2004-27 July 2007. Electron flux data were obtained from the
98 HEO-3 satellite which lies in a roughly 12 hour highly elliptical orbit with good data coverage in the L
99 range from 2 to 9 (Fennell et al., 2004; Fennell and Roeder, 2008). The orbit is such that it cycles
100 through all MLT. We use the E2 telescope channel (>0.23 MeV) and the omnidirectional sensors E4-E6
101 channels (>0.6 , > 1.5 , and > 2.9 MeV) (all sampling number of electrons/second) with observations
102 binned by L shell (IGRF) with, for example, $L=2$ including $L=2.0-2.99$. The E2 telescope temperature rose
103 with altitude at $L \geq 5$ which increased noise levels. This may mean that results in the >0.23 MeV channel
104 at higher L are less reliable. We use only data collected over the northern hemisphere (high altitude)
105 where dwell time at each L shell is longer. This reduced variability in the data as pitch angles differ
106 between northern and southern hemispheres. We did, however, retain both "even" and "odd" orbits,
107 which sample different MLT, to obtain a more representative average of the electron population. Note
108 that L is correlated with latitude, with lower L shells ($L \leq 3$) sampled from near the equator. As high
109 energy protons can contaminate the electron channels, we removed days on which solar proton events
110 were occurring, as well as one day following (<ftp://ftp.swpc.noaa.gov/pub/indices/SPE.txt>). However,
111 there may also be proton contamination outside solar proton events. To correct for this, we removed

112 data falling far above the cloud of data points when proton vs. electron counts are plotted (O'Brien,
113 2012). This removed more lower L shell observations ($L < 4$). For this reason, results from lower L shells
114 are not as robust.

115 We obtained VLF power spectral density ($\log_{10} [\mu V^2 / m^2 / Hz]$) from dayside, northern hemisphere
116 passes (LT 10:30) from the Instrument Champ Electrique (ICE) on the DEMETER satellite (Berthelier et
117 al., 2006). There was good data coverage over $L=1-6$ (IGRF). We limit the VLF data to the lower band
118 chorus range (0.1-0.5 fce). We expect this dataset is likely dominated by lower band chorus activity, but
119 acknowledge that other VLF wave activity could be present. Therefore, more generally, this dataset
120 contains whistler mode waves. In particular, this VLF wave band at lower L shells (within the
121 plasmasphere) is dominated by hiss (Bortnik et al., 2008). Chorus waves predominate above the
122 plasmopause ($L \sim 3$) and hiss within the plasmasphere below this (Carpenter and Park, 1973). We use only
123 the dayside pass of the satellite because this range of VLF is found over a broader range of latitudes on
124 dayside rather than nightside and is not as influenced by geomagnetic activity (Tsurutani & Smith, 1977;
125 Li et al., 2009, Thorne et al., 2010). This may represent only a sample of overall global activity as
126 satellites can only sample one small area of the magnetosphere at a time. In particular, it may result in a
127 certain L shell being more heavily sampled at a particular local time.

128 ULF Pc3, Pc4, and Pc5 wave power (nT^2/Hz) was obtained from individual McMAC ground stations at
129 $L=2.5$ (Bennington or BENN) and $L=3.4$ (Glyndon or GLYN) and CARISMA ground stations at $L=4.06$
130 (Pinawa or PINA), $L=5.15$ (Island Lake or ISLL), $L=6.15$ (Gillam or GILL), and $L=7.44$ (Fort Churchill or
131 FCHU). Wave power was calculated using a Fourier transform with a 1 h window. This allows a good
132 discernment of waves down to the minimum (Pc5) frequency of 1.67 mHz. There were strong
133 correlations between the 3 ULF wave bands at all the ground stations, and each band correlated
134 extremely similarly with electron flux. In order to compare most easily to the ULF index, we use Pc5 in
135 most of our analyses, however, given the high correlations between bands, each of Pc3, Pc4, and Pc5 are
136 a nearly identical proxy for the other two. Daily averaged ULF Pc5 wave power was obtained from a
137 ground-based ULF Pc5 index covering local times 0500 – 1500 in the Pc5 range (2-7 mHz) obtained from
138 magnetometers stationed at 60-70° N CGM (Corrected GeoMagnetic) latitude (Kozyreva et al., 2007).

139 The log values of lower band chorus PSD, ULF power, and flux data were all daily averaged. Predictor
140 variables (VLF and ULF wave activity) were lagged at 0 (same day; Lag 0), 1 (previous day; Lag 1), 2, and 3
141 days as most of the correlation between these waves and electron flux occurs within this time frame
142 (Mann et al., 2004; Simms et al., 2018a). For the correlation and regression analyses, daily change in
143 electron flux was calculated by subtracting the daily average of the previous day from the current day's
144 average. All single correlations reported are standard Pearson correlation coefficients. Partial
145 correlation between two factors fixes other variables at a given level to control for their effects (Neter et
146 al., 1985).

147 The flux observations show serial autocorrelation ($p < 0.0001$ using Durbin-Watson test, see Neter et al.,
148 1985), as each day is correlated with the previous day. To correct for this, we include previous day's flux
149 as a predictor in the regression models. The result of this is that the regressions are essentially AR1
150 (autoregressive at one time step, represented by the previous day's flux term) differenced (as the
151 observations are daily change) models (Hyndman and Athanasopoulos, 2018; Simms et al., 2019). The
152 addition of the AR1 term reduces the autocorrelation enough that we can have confidence in the p-
153 values of the statistical tests. Nonlinear effects of waves on electron flux are explored by including
154 quadratic terms in the regression analyses, while the synergistic combined action of ULF and VLF waves
155 is tested by including a multiplicative term (Neter et al., 1985).

156 Statistical analyses were performed in MATLAB.

157

158 3. Results

159 Daily average electron fluxes peak at L=4, with lower values observed in the slot region (L=2) and
160 beyond geosynchronous orbit (L>6) (Figure 1). In contrast, \log_{10} lower band chorus PSD (from DEMETER
161 satellite) increases steadily up to L=6 (Figure 2).

162 The power of all three ULF bands from the ground stations (Pc3, Pc4, and Pc5) rise over L=2-6, with very
163 low power seen at L2 (Figure 3). ULF Pc4 has the highest power, but there are such high correlations
164 between these three bands (0.9432 - 0.9989) that any band is an almost exact proxy for the other two.

165

166 3.1 Correlations between Chorus PSD and Electron Flux

167 Neither hiss nor chorus PSD on the same day (Lag 0) is strongly associated with electron flux difference
168 at >1.5 MeV with correlations ranging from -0.02 to 0.07 (Table 1). When chorus is measured the day
169 before (Lag 1), there are stronger correlations at L>3, but all are below 0.40 (Figure 4; Table 1).

170

171 Table 1. Correlation of same day (Lag 0) and previous day (Lag 1) hiss (L<4) and chorus (L>3) PSD with
172 >1.5 MeV electron flux daily change.

L shell	Same day (Lag 0)	Day previous (Lag 1)
L=2-2.99	0.04	0.03
L=3-3.99	0.07	0.15
L=4-4.99	-0.02	0.37
L=5-5.99	-0.02	0.35
L=6-6.99	-0.05	0.30

173

174 Both VLF in the chorus band and flux differences show little spread below L=3. Values are tightly
175 clustered at low VLF PSD (not much VLF is seen at these L shells) and around 0 change in electrons. This
176 may reduce the likelihood of seeing much influence of the VLF whistler mode waves on changes in
177 electron flux at L=2-2.99.

178 We perform partial correlations between VLF waves at each L shell (2-6) over 0-3 days with daily flux
179 difference at the four energy levels (Figure 5, $r < 0.10$ lie within the gray band). At L=2-2.99 (hiss), nearly
180 all correlation magnitudes were less than 0.1. Over L=4-5, chorus measured on the same day is
181 associated with a drop in flux at the 3 higher energies. Chorus measured one day before (Lag 1) is most
182 associated with an increase in flux at all 4 energies over L=4-6. However, none of the correlations
183 exceed 0.4. These low correlations suggest that the chorus is not the only driver of electron changes.
184 However, we note that the partial correlation analysis differentiates the Lag 0 effect more clearly than
185 the simple correlation analysis of Table 1. Over L=4-5, at >1.5 MeV, electron reductions at Lag 0 due to
186 chorus are stronger (L4: $r = -0.32$, L5: $r = -0.21$ in the partial correlations). The Lag 1 partial correlation
187 with flux enhancement is more similar (L4: $r = 0.38$, L5: $r = 0.35$ in the >1.5 MeV partial correlations) to
188 that found with simple correlation.

189

190

191 3.2 Correlations between ULF Power and Electron Flux

192 Despite the obvious differences in power, extremely high correlations (0.9432 - 0.9989) between the
193 three ULF bands (Pc3, Pc4, and Pc5) suggest that any one could serve as an excellent proxy for the
194 others. Simple correlations between each ULF band (Lag 1) and >1.5 MeV electron flux at L=5 are
195 identical (Figure 6). Partial correlations over 0-3 days previous between ULF in each band with the daily
196 differences in the 4 electron flux energies at L = 5 show this to be the case (Figure 7). The pattern of
197 correlation was virtually the same between each ULF band and electron flux. These correlations were
198 similarly indistinguishable at the other L shells. We continue our analysis using ULF Pc5 data.

199
200 ULF power shows a similar pattern to that of the effect of chorus (or hiss at the lower L shells) on >1.5
201 MeV flux: Lag 1 correlations tend to be positive and of greater magnitude than Lag 0 correlations. Both
202 Lag 0 and Lag 1 correlations are greatest in magnitude over L=4-7 (Table 2; Figure 8). ULF Pc5 at L=5 is
203 the most highly correlated (r=0.34).

204
205 Table 2. Correlation of same day (Lag 0) and previous day (Lag 1) ULF Pc5 power with >1.5 MeV electron
206 flux daily change.

L shell	a. Same day (Lag 0)	b. Day previous (Lag 1)
L=2 (BENN)	0.05	0.06
L=3 (GLYN)	0.06	0.19
L=4 (PINA)	-0.19	0.33
L=5 (ISLL)	-0.19	0.34
L=6 (GILL)	-0.20	0.30
L=7 (FCHU)	-0.20	0.18

207 Partial correlations of ULF power at each L shell (1-7) with the flux differences over 0-3 day lags show a
208 similar pattern to that of VLF waves (Figure 9). At L=2, all correlations were low (close to or less
209 than |0.1|). At L=3, the most important ULF correlations are at Lag 1, but these are all ≤ 0.25 . Over L=4-
210 7, the peak in positive association occurs with previous day's ULF, while the strongest negative
211 correlations are with Lag 0 ULF. Using partial correlation analysis, we can more clearly see the electron
212 decreases at Lag 0 associated with ULF waves than the individual correlations of Table 2 would suggest.
213 The middle range of flux energies (>0.6 MeV and >1.5 MeV) show the highest response (r as low as -0.4
214 at Lag 0 and as high as 0.4 at Lag 1). ULF power from 2 days previous is less associated with flux changes
215 and that from 3 days prior is below |0.10|.

216
217 3.3 The ULF Index Is a Reasonable Proxy for ULF Pc5 Power at Each L Shell

218 If ULF power measurements from each L shell are not available, the ULF index can be a practical
219 replacement. The correlation of the index with ULF Pc5 power at ground stations at each L shell is
220 reasonably high (0.74 – 0.85, Table 3a). The correlation of daily change of electron flux at each L shell
221 with the Lag 1 index is also very similar to that with each ground station, despite not being centered on
222 a particular L shell (compare Table 2b with Table 3b).

223
224 Table 3. At each L shell, the correlation of the ULF Pc5 index a. with ULF Pc5 power at individual
225 CARISMA ground stations and b. with next day's >1.5 MeV electron flux daily change.

L shell	a. ULF Index with ground station	b. Electron flux with Lag 1 ULF Index
L=2	0.74	0.05
L=3	0.83	0.19
L=4	0.85	0.38
L=5	0.80	0.33
L=6	0.78	0.24
L=7	0.76	0.13

226

227

228

229

230 3.4 Combined Effects of Chorus and ULF Pc5

231 A key question is whether the two most important factors, chorus (at $L > 3$) and ULF Pc5, each still
 232 correlate with flux changes when the other factor is accounted for. To determine this, we perform
 233 multiple regressions including both wave types, producing standardized regression coefficients so as to
 234 compare relative strengths of predictors on a common scale. As the highest partial correlations were
 235 on Lag 0-2 (same day to two days previous) we include all these measures over $L=3-6$, the L shells in
 236 which both chorus and ULF power have good data coverage and where the individual correlations with
 237 flux were highest. Previous day's flux (Lag 1 daily flux change) is included as a predictor in the model to
 238 correct for serial autocorrelation (leading to an essentially AR1 model).

239 Over $L=4-6$, ULF Pc5 consistently shows a stronger influence than chorus over Lag 0-1, with a negative
 240 influence at Lag 0 and positive influence at Lag 1 (Figure 10; red line indicates statistically significant
 241 coefficients). It is notable that the influence of ULF Pc5 Lag 2 increases from low to high flux energy
 242 levels, while that at Lag 1 decreases. This indicates that it takes up to several days for processes driven
 243 by these waves to accelerate electrons up to the higher energies. At the 3 highest energies, ULF Pc5
 244 influence at each time step is strongest at $L=4$ (decreasing through $L=6$) and at >0.6 MeV flux (decreasing
 245 up to >2.9 MeV). At $L=3$, Lag 1 ULF is also much more important than chorus. However, there is more
 246 effect of chorus at Lag 0 at the higher 2 energies, and the ULF correlation is positive at the 2 lower
 247 energies.

248 This combined variable set (lags 0-2 of both chorus and ULF and previous day's flux) is most strongly
 249 associated with flux differences at >1.5 MeV. R^2 (percent of variability in the data explained by the
 250 regression model) peaks at 47.1% at $L=5$ in the >1.5 MeV energy range. This corresponds roughly to a
 251 correlation of 0.69 (the square root of R^2). However, the variability explained is not much lower at the
 252 other 3 energies. The rough correlation estimate is similar at >0.6 and >2.9 MeV ($r = 0.66$ and 0.65), but
 253 somewhat lower at >0.23 MeV (0.58). At each L shell and energy, the correlation of flux with chorus and
 254 ULF Pc5 combined is higher than in the simple correlations. This indicates that both factors and all lags
 255 are needed for a fuller description of flux changes.

256

257 3.5 Nonlinear Effects of Chorus and ULF Pc5 on Flux

258 However, these linear, additive models may not completely capture the combined effects of chorus and
259 ULF waves on electron flux. The effect of each factor may be neither linear nor independent of the
260 other wave type. For each of Lag 0 and 1, we include squared terms to describe nonlinear effects, and a
261 multiplicative interaction term to describe possible synergistic effects between the chorus and ULF wave
262 effects. Regression surfaces show the predicted combined response of flux difference to both wave
263 types with the marginal effects shown by the slope of the surface at each edge. The marginal effect is
264 the effect of one predictor variable when the other predictor is held constant at 0.

265 When waves are measured on the same day as flux change (Lag 0) chorus and ULF waves appear to act
266 independently. There is no strong multiplicative interaction visible in the surface plots (Figure 11). Over
267 L 4-5, at the three higher energies, the linear response to ULF power is negative with an increasingly
268 negative response at higher ULF power (the nonlinear term). In contrast, at L=3, ULF is associated with
269 flux increases, particularly at the lower energies. (This can also be seen in the regression coefficients of
270 Figure 10.) The response to VLF waves is linear and positive over L=4-6.

271 However, a synergistic action is seen between wave types at Lag 1 at the three highest energies (Figure
272 12). Flux responds more positively to the highest chorus or ULF levels when the other wave type is also
273 at a high level. This can be seen on the surface plots in the unexpected rise in flux difference in the
274 farthest corner (black arrows in 12b mark some of the strongest examples of this). However, as much of
275 the chorus and ULF individual effects may be explained by their action within this multiplicative
276 interaction term, the remaining individual marginal effects may appear negative (blue and orange
277 arrows of 12b). This is most notable with chorus and suggests that much of the positive effect of chorus
278 is the result of joint action with ULF waves rather than from its own individual, additive effects.
279 Increased electron flux, therefore, may be the result of a combination of processes driven by ULF and
280 chorus waves. Flux enhancement is less likely to occur when either wave type occurs alone. Although
281 the nonlinear component of chorus waves still tends to result in flux decreases, ULF waves show some
282 positive, nonlinear effects, with the highest ULF power resulting in higher flux increases (green arrow of
283 12b).

284

285 4. Discussion

286 In this study, we find that chorus and ULF waves are most explanatory of relativistic flux changes over
287 L=4-6, with their strongest influence seen on the >1.5 MeV electrons. Reductions and enhancements of
288 flux due to these waves occur at different time scales, with decreases occurring near simultaneously
289 with increased wave activity, while enhancement, particularly of higher energy electrons due to ULF
290 waves, occurs over a longer time scale.

291 When measured on the same day as flux (Lag 0), chorus (above L=3) and ULF waves predict electron
292 decreases (at >0.6 MeV and above). There was little association between flux changes at higher
293 energies and Lag 0 hiss (below L=4), although we note a weak positive correlation at L=3 in the >0.23
294 flux band. We assume these decreases may represent electron loss. This short timescale has been
295 previously noted for VLF waves: loss due to scattering by chorus or hiss occurs at < 1 day (Summers et
296 al., 2007) and within the plasmasphere (Jaynes et al., 2014).

297 However, when measured on the previous day (Lag 1), these waves are associated with flux
298 enhancements on the following day, consistent with previous observations of chorus (at L>3) and hiss
299 (below L=3) (Summers et al., 2007), as well as ULF influences on electron flux around 1 MeV (Elkington

300 et al., 1999). Peak correlations between ULF waves and electron flux have been noted at a lag of 2-3
301 days (Mann et al., 2004). Our use of partial correlation analysis has refined the peak of the
302 enhancement correlation to a one day lag by removing the loss influences that occur more immediately.

303 Over L=4-6, ULF Pc5 wave activity from two days previous (Lag 2) is also influential at higher L shells
304 and/or at higher electron energies. At Lag 2 (waves measured two days before flux), above L=3, the
305 influence of ULF Pc5 increases from low to high electron energy levels, while that of the Lag 1 response
306 drops off. Enhancement processes due to ULF waves, therefore, appear to energize electrons in stages,
307 bringing them from lower to the highest energies over a period of days, a response that has been noted
308 previously to geomagnetic indices and solar wind speed (Rodger et al., 2010). This trend was seen for
309 chorus influences as well over L=4-5, but it is much less marked. It is also notable that the Lag 2 ULF
310 influence increases at higher L shells, while the influence of VLF waves drops off. The implications of
311 these trends are that inward radial diffusion, driven by ULF waves, takes some time (> 1 day) to bring
312 electrons to the higher energies, that radial diffusion is of more importance at L>3 with increasing
313 influence at higher L shells, and that local acceleration due to VLF waves is only an important factor at
314 L<5.

315
316 We note that L shell and latitude are correlated in the HEO-3 dataset, resulting in a correlation between
317 pitch angle and L shell. As wave action may depend on pitch angle, this may be at least part of the
318 reason behind the correlational differences seen between flux changes and waves at different L shells
319 (Shprits et al., 2008).

320
321 Previously, it was suggested that electron flux peaks are due to both VLF/ELF and ULF acceleration
322 equally near L=4.5, but to ULF acceleration alone at and above geosynchronous orbit (O'Brien et al.,
323 2003). However, we have here found that the association of ULF waves with flux changes is stronger
324 than that with VLF waves at all L shells studied (at Lag 1). Although we note that the chorus (VLF) effect
325 is strongest relative to the ULF correlation at L=4, its standardized regression coefficient is still always
326 less than the corresponding ULF coefficient. This difference in relative effect of VLF vs. ULF between
327 studies may result from our use of satellite-observed VLF data which is a more accurate depiction of
328 chorus rather than the microburst proxy data used in the previous study. However, there are other
329 differences. We do not analyze flux changes solely following storms, choosing instead to measure daily
330 changes; we use multiple regression to statistically determine the simultaneous effects of VLF and ULF;
331 and the levels of geomagnetic activity between our time period of study (2004-2007) and that of the
332 previous paper (1996-2001) are dissimilar. All these differences may contribute to finding a stronger
333 relative enhancement effect of ULF waves over L=3-6.

334 Above L=3, electron decreases (at Lag 0) are more strongly associated with ULF Pc5 wave activity than
335 with chorus. This has been previously observed in several storms (Katsavrias et al., 2015), but we show
336 this with a statistical analysis here. We also show that there is some contribution to electron reductions
337 from chorus, presumably due to scattering of electrons into the loss cone. The strongest effect of
338 chorus on electron decreases occurs at the highest electron energy (>2.9 MeV), with the influence
339 dropping at each higher L shell.

340

341

342 4.1 Nonlinear influences of ULF and VLF wave activity

343 While at Lag 1 the linear regression model shows ULF Pc5 wave power is more strongly associated with
344 flux changes than chorus, the addition of nonlinear (quadratic) and interaction (multiplicative) terms
345 describes a more nuanced relationship. Flux enhancement is more likely when both chorus and ULF
346 waves are high. Their action is more effective in combination than when alone. This was found
347 previously for electrons at geosynchronous orbit (Simms et al., 2018b) but we now confirm this finding
348 for lower L shells. Not all associations between flux change and wave activity are linear when the
349 multiplicative interaction term is included in the model, nor are they all positive. These marginal
350 (individual) negative responses in the nonlinear models result from much of the flux response being tied
351 up in the multiplicative interaction term. They are what is left over after the more significant, and
352 positive, interactive effect is accounted for. This argues that the processes associated with chorus (local
353 acceleration) and those associated with ULF waves (inward radial diffusion) are both necessary to
354 produce flux enhancements and do not act independently. This is consistent with the proposed two-
355 step process where local acceleration by chorus waves first energizes electrons which are then brought
356 to even higher energies by inward radial diffusion (Jaynes et al., 2015; Katsavrias et al., 2019; Zhao et al.,
357 2019).

358 The same cannot be said for flux decreases on the same day (Lag 0 analyses; L 4-6). In this case, chorus
359 and ULF waves act independently. There is no strong multiplicative interaction visible in the surface
360 plots. Those processes associated with loss due to chorus (which scatters electrons into the loss cone)
361 and ULF waves (via outward radial diffusion) are able to operate independently. There is some
362 nonlinearity to the flux response to ULF waves with a stronger decrease in flux at high ULF in the lowest
363 energies and less decrease in flux at high ULF in the higher energies.

364

365

366

367

368 5. Summary

369 a. We use multiple regression to control for the effects of other variables and to determine
370 the timescale of electron decreases vs. enhancement. By holding other factors constant
371 in this way, we see that the individual effects on electron reductions and enhancements
372 due to chorus and ULF waves are often stronger than it would appear from individual
373 correlations.

374

375 b. Over L=4-6 (4.0-6.99), both chorus and ULF Pc5 drive immediate electron decreases and
376 delayed enhancement.

377

378 c. ULF waves consistently show a stronger influence on electron enhancement than do
379 chorus waves. ULF power is also often more associated with electron reductions than
380 chorus.

381

382 d. There is a synergistic interaction between chorus and ULF wave activity on electron
383 enhancement. This means that their combined effect is stronger than would be

384 expected. This points to a two-step process of electron acceleration where local
385 acceleration by chorus waves energizes electrons which are subsequently brought to
386 even higher energies by inward radial diffusion.

387
388 e. However, chorus and ULF waves drive electron decreases additively. In other words, the
389 actions of the two wave types act independently.

390
391 f. Contributions of ULF Pc5 and what are likely hiss to electron decreases and
392 enhancement are lower at $L < 4$ than at $L \geq 4$, and minimal at $L = 2$.

393

394

395 Acknowledgements

396 We thank T.P. O'Brien for suggesting this study, advice, and for providing electron data from the HEO-3
397 satellite (data available at: <http://virbo.org/HEO>). We thank R. Gamble for preparing and J.-J. Berthelier
398 for providing DEMETER ICE data, available at the CDPP (Centre de données de la Physique des Plasmas)
399 website: <https://cdpp-archive.cnes.fr/>. CARISMA data are available at
400 <https://www.carisma.ca/carisma-data-repository>. McMAC data can be accessed through the CDAWeb
401 at <https://cdaweb.sci.gsfc.nasa.gov/index.html/>. The ULF Pc5 index is available at
402 http://ulf.gcras.ru/plot_ulf.html. The suggestions of an anonymous reviewer greatly improved this
403 manuscript.

404 Work at Augsburg University was supported by NSF grant AGS-1651263.

405

406 Literature Cited

407

408 Berthelier, J. J., Godefroy, M., Leblanc, F., Malingre, M., Menvielle, M., Lagoutte, D., et al. (2006). ICE,
409 the electric field experiment on DEMETER. *Planetary and Space Science*, 54(5), 456-471,
410 <https://doi.org/10.1016/j.pss.2005.10.016>

411
412 Blake, J. B., D. N. Baker, N. Turner, K. W. Ogilvie, and R. P. Lepping (1997), Correlation of changes in the
413 outer-zone relativistic-electron population with upstream solar wind and magnetic field measurements,
414 *Geophysical Research Letters*, 24, 927, doi.org/10.1029/97GL00859

415

416 Carpenter, D.L. and C. G. Park (1973), On what ionospheric workers should know about the
417 plasmopause-plasmasphere, *Reviews of Geophysics*, 11, 133,
418 <https://doi.org/10.1029/RG011i001p00133>

419

420 Claudepierre, S. G., I. R. Mann, K. Takahashi, J. F. Fennell, M. K. Hudson, J. B. Blake, J. L. Roeder, J. H.
421 Clemmons, H. E. Spence, G. D. Reeves, D. N. Baker, H. O. Funsten, R. H. W. Friedel, M. G. Henderson,

422 C. A. Kletzing, W. S. Kurth, R. J. MacDowall, C. W. Smith, and J. R. Wygant (2013), Van Allen Probes
423 observation of localized drift resonance between poloidal mode ultra-low frequency waves and 60 keV
424 electrons, *Geophysical Research Letters*, 40, 4491–4497, doi:10.1002/grl.50901.
425

426 Clilverd, M A, C J Rodger, M Andersson, P T Verronen, and A Seppälä (2016), Linkages between the
427 radiation belts, polar atmosphere and climate: electron precipitation through wave particle interactions,
428 in *Waves, particles and storms in geospace*, edited by Georgios Balasis, Ioannis A. Daglis, and Ian R.
429 Mann, Chapter 14, 355-376, Oxford University Press,
430 <http://dx.doi.org/10.1093/acprof:oso/9780198705246.003.0015>, ISBN: 9780198705246
431

432 Elkington, S.R., M.K. Hudson, A. A. Chan (1999), Acceleration of relativistic electrons via drift-resonant
433 interaction with toroidal-mode Pc-5 ULF oscillations, *Geophysical Research Letters*, VOL. 26, NO. 21,
434 3273-3276, doi.org/10.1029/1999GL003659
435

436 Fennell J.F., J. B. Blake, R. Friedel, and S. Kanekal (2004), The Energetic Electron Response to Magnetic
437 Storms: HEO Satellite Observations, Aerospace Report No. TR-2004(8570)-5
438

439 Fennell, J. F. and J. Roeder (2008), Storm time phase space density radial profiles of energetic electrons
440 for small and large K values: SCATHA results, *Journal of Atmospheric and Solar-Terrestrial Physics*
441 70(14):1760-1773, doi: 10.1016/j.jastp.2008.03.014
442

443 Hao, Y. X., Q.-G. Zong, Y. F. Wang, X.-Z. Zhou, Hui Zhang, S. Y. Fu, Z. Y. Pu, H. E. Spence,
444 J. B. Blake, J. Bonnell, J. R. Wygant, and C. A. Kletzing (2014), Interactions of energetic electrons with
445 ULF waves triggered by interplanetary shock: Van Allen Probes observations in the magnetotail, *Journal*
446 *of Geophysical Research Space Physics*, 119, 8262–8273, doi:10.1002/2014JA020023.
447

448 Hao, Y. X., Zong, Q.-G., Zhou, X.-Z., Rankin, R., Chen, X. R., Liu, Y., et al. (2019). Global-scale ULF waves
449 associated with SSC accelerate magnetospheric ultrarelativistic electrons. *Journal of Geophysical*
450 *Research: Space Physics*, 124, 1525–1538. <https://doi.org/10.1029/2018JA026134>
451

452 Horne, R. B., and R. M. Thorne (2003), Relativistic electron acceleration and precipitation
453 during resonant interactions with whistler-mode chorus, *Geophysical Research Letters*, 30(10), 1527,
454 doi:10.1029/2003GL016973
455

456 Horne, R. B., R. M. Thorne, S. A. Glauert, J. M. Albert, N. P. Meredith, and R. R. Anderson (2005),
457 Timescale for radiation belt electron acceleration by whistler mode chorus waves, *Journal of*
458 *Geophysical Research*, 110, A03225, doi:10.1029/2004JA010811
459

460 Hyndman, R.J., & Athanasopoulos, G. (2018) *Forecasting: principles and practice*, 2nd edition, OTexts:
461 Melbourne, Australia. OTexts.com/fpp2
462

463 Jaynes, A.N., X. Li, Q.G. Schiller, L.W. Blum, W. Tu, D.L. Turner, B. Ni, J. Bortnik, D.N.
464 Baker, S.G. Kanekal, J.B. Blake and J. Wygant (2014), Evolution of relativistic outer
465 belt electrons during an extended quiescent period, *Journal of Geophysical Research*, 119, 9558–9566,
466 doi:10.1002/2014JA020125.
467

468 Jaynes, A. N., et al. (2015), Source and seed populations for relativistic electrons: Their roles in radiation
469 belt changes, *Journal of Geophysical Research Space Physics*, 120, 7240–7254,
470 doi:10.1002/2015JA021234.
471

472 Katsavrias, C., I. A. Daglis, W. Li, S. Dimitrakoudis, M. Georgiou, D. L. Turner, and C. Papadimitriou,
473 (2015), Combined effects of concurrent Pc5 and chorus waves on relativistic electron dynamics, *Annales*
474 *Geophysicae*, 33, pp 1173–1181, doi:10.5194/angeo-33-1173-2015.
475

476 Katsavrias, C., Sandberg, I., Li, W., Podladchikova, O., Daglis, I. A., Papadimitriou, C., et al. (2019). Highly
477 relativistic electron flux enhancement during the weak geomagnetic storm of April–May 2017. *Journal of*
478 *Geophysical Research: Space Physics*, 124, 4402–4413. <https://doi.org/10.1029/2019JA026743>
479

480 Kellerman, A. C., and Y. Y. Shprits (2012), On the influence of solar wind conditions on the outer-electron
481 radiation belt, *Journal of Geophysical Research*, 117, A05217, doi:10.1029/2011JA017253.
482

483 Kozyreva, O., V. Pilipenko, M. J. Engebretson, K. Yumoto, J. Watermann, and N. Romanova (2007), In
484 search of a new ULF Pc5 wave index: Comparison of Pc5 power with dynamics of geostationary
485 relativistic electrons, *Planetary Space Science*, 55, 755–769.
486

487 Li, L., J. Cao, and G. Zhou (2005), Combined acceleration of electrons by whistler-mode and
488 compressional ULF turbulences near the geosynchronous orbit, *Journal of Geophysical Research*, 110,
489 A03203, doi:10.1029/2004JA010628.
490

491 Li, W., R. M. Thorne, V. Angelopoulos, J. Bortnik, C. M. Cully, B. Ni, O. LeContel, A. Roux, U. Auster, and
492 W. Magnes (2009), Global distribution of whistler-mode chorus waves observed on the THEMIS
493 spacecraft, *Geophysical Research Letters*, 36, L09104, doi:10.1029/2009GL037595.
494

495 Loto'aniu, T., Thorne, R., Fraser, Brian, & Summers, D. (2006). Estimating relativistic electron pitch angle
496 scattering rates using properties of the electromagnetic ion cyclotron wave spectrum. *Journal of*
497 *Geophysical Research*. 111. 10.1029/2005JA011452
498

499 Loto'aniu, T. M., H. J. Singer, C. L. Waters, V. Angelopoulos, I. R. Mann, S. R. Elkington, and J. W. Bonnell
500 (2010), Relativistic electron loss due to ultralow frequency waves and enhanced outward radial
501 diffusion, *Journal of Geophysical Research*, 115, A12245, doi:10.1029/2010JA015755
502

503 Mann, I.R., T.P. O'Brien, D.K. Milling (2004), Correlations between ULF wave power, solar wind speed,
504 and relativistic electron in the magnetosphere: solar cycle dependence, *Journal of Atmospheric and*
505 *Solar-Terrestrial Physics* 66 (2004) 187– 198, doi:10.1016/j.jastp.2003.10.002
506

507 Mann, I. R., Murphy, K. R., Ozeke, L. G., Rae, I., Milling, D. K., and Kale, A. (2012), The role of ultralow
508 frequency waves in radiation belt dynamics, *Geoph. Monog. Series*, 199, 69–92,
509 doi:10.1029/2012GM001349
510

511 Neter, J., Wasserman, W., & Kutner, M. H. (1985). *Applied linear statistical models*, (p. 1127).
512 Homewood, Ill: Richard D. Irwin, Inc.
513

514 O'Brien, T. P., K. R. Lorentzen, I. R. Mann, N. P. Meredith, J. B. Blake, J. F. Fennell, M. D. Looper, D. K.
515 Milling, and R. R. Anderson (2003), Energization of relativistic electrons in the presence of ULF power
516 and MeV microbursts: Evidence for dual ULF and VLF acceleration, *Journal of Geophysical Research*,
517 108(A8), 1329, doi:10.1029/2002JA009784
518

519 O'Brien, T.P. (2012), Data Cleaning Guidelines for AE-9/AP-9 Datasets, Aerospace Report No. TOR-
520 2012(1237)-4
521

522 Ozeke, L. G., Mann, I. R., Dufresne, S. K. Y., Olifer, L., Morley, S. K., Claudepierre, S. G., et al. (2020).
523 Rapid outer radiation belt flux dropouts and fast acceleration during the March 2015 and 2013 storms:
524 The role of ULF wave transport from a dynamic outer boundary. *Journal of Geophysical Research: Space*
525 *Physics*, 125, e2019JA027179. <https://doi.org/10.1029/2019JA027179>
526

527 Reeves, G. D., et al. (2013), Electron acceleration in the heart of the Van Allen radiation belts, *Science*,
528 341, 999–994, doi:10.1126/science.1237743
529

530 Rodger, C. J., Clilverd, M. A., Green, J. C., and Lam, M. M. (2010), Use of POES SEM-2 observations to
531 examine radiation belt dynamics and energetic electron precipitation into the atmosphere, *J. Geophys.*
532 *Res.*, 115, A04202, doi:10.1029/2008JA014023
533

534 Shprits, Y.Y., Subbotin, D.A., Meredith, D.P., Elkington, S.R. (2008), Review of modeling of losses and
535 sources of relativistic electrons in the outer radiation belt II:Local acceleration and loss, *Journal of*
536 *Atmospheric and Solar-Terrestrial Physics*,70:1694–1713, doi:10.1016/j.jastp.2008.06.014
537

538 Shprits, Y. Y., Thorne, R. M., Friedel, R., Reeves, G. D., Fennell, J., Baker, D. N., and Kanekal, S. G. (2006),
539 Outward radial diffusion driven by losses at magnetopause, *Journal of Geophysical Research*, 111,
540 A11214, doi:10.1029/2006JA011657
541

542 Shprits, Y. Y., Meredith, N. P., and Thorne, R. M. (2007), Parameterization of radiation belt electron loss
543 timescales due to interactions with chorus waves, *Geophysical Research Letters*, 34, L11110,
544 doi:10.1029/2006GL029050
545

546 Shprits, Y. Y., A. Kellerman, N. Aseev, A. Y. Drozdov, and I. Michaelis (2017), Multi-MeV electron loss in
547 the heart of the radiation belts, *Geophysical Research Letters*, 44, 1204–1209,
548 doi:10.1002/2016GL072258.
549

550 Simms, L., Engebretson, M., Clilverd, M., Rodger, C., Lessard, M., Gjerloev, J., & Reeves, G. (2018a). A
551 distributed lag autoregressive model of geostationary relativistic electron fluxes: Comparing the
552 influences of waves, seed and source electrons, and solar wind inputs. *Journal of Geophysical Research:*
553 *Space Physics*, 123. <https://doi.org/10.1029/2017JA025002>
554

555 Simms, L. E., Engebretson, M. J., Clilverd, M. A., Rodger, C. J., & Reeves, G. D. (2018b). Nonlinear and
556 synergistic effects of ULF Pc5, VLF chorus, and EMIC waves on relativistic electron flux at
557 geosynchronous orbit. *Journal of Geophysical Research: Space Physics*, 123. [https://doi.](https://doi.org/10.1029/2017JA025003)
558 [org/10.1029/2017JA025003](https://doi.org/10.1029/2017JA025003)
559

560 Simms, L. E., Engebretson, M. J., Clilverd, M. A., & Rodger, C. J. (2019). Ground-based observations of
561 VLF waves as a proxy for satellite observations: Development of models including the influence of solar
562 illumination and geomagnetic disturbance levels. *Journal of Geophysical Research: Space Physics*,
563 124, 2682–2696. <https://doi.org/10.1029/2018JA026407>
564

565 Summers, D., R.M. Thorne, and F. Xiao (1998), Relativistic theory of wave-particle resonant diffusion
566 with application to electron acceleration in the magnetosphere, *Journal of Geophysical Research*, 103,
567 20,487-20,500, <https://doi.org/10.1029/98JA01740>
568

569 Summers, D., B. Ni, and N. P. Meredith (2007), Timescales for radiation belt electron acceleration and
570 loss due to resonant wave-particle interactions: 2. Evaluation for VLF chorus, ELF hiss, and
571 electromagnetic ion cyclotron waves, *Journal of Geophysical Research*, 112, A04207,
572 doi:10.1029/2006JA011993.
573

574 Tan, L. C., X. Shao, A. S. Sharma, and S. F. Fung (2011), Relativistic electron acceleration by
575 compressional-mode ULF waves: Evidence from correlated Cluster, Los Alamos National Laboratory
576 spacecraft, and ground-based magnetometer measurements, *Journal of Geophysical Research*, 116,
577 A07226, doi:10.1029/2010JA016226.
578

579 Thorne, R.M. (2010), Radiation belt dynamics: The importance of wave-particle interactions, *Geophysical*
580 *Research Letters*, 37, L22107, doi:10.1029/2010GL044990.

581

582 Thorne, R. M., T. P. O'Brien, Y. Y. Shprits, D. Summers, and R. B. Horne (2005), Timescale for MeV
583 electron microburst loss during geomagnetic storms, *Journal of Geophysical Research*, 110, A09202,
584 doi:10.1029/2004JA010882.

585 Tsurutani, B. T. and Edward J. Smith (1977), Two types of magnetospheric ELF chorus and their substorm
586 dependences, *Journal of Geophysical Research*, 82, 5112-5128, doi: 10.1029/JA082i032p05112.

587

588 Turner, D. L., Shprits, Y., Hartinger, M., and Angelopoulos, V. (2012), Explaining sudden losses of outer
589 radiation belt electrons during geomagnetic storms, *Nature Physics Lett.*, 8, 208–212,
590 doi:10.1038/NPHYS2185
591

592 Turner, D. L., et al. (2017), Investigating the source of near-relativistic and relativistic electrons in Earth's
593 inner radiation belt, *Journal of Geophysical Research Space Physics*, 122, 695–710,
594 doi:10.1002/2016JA023600.
595

596 Usanova, M. E., et al. (2014), Effect of EMIC waves on relativistic and ultrarelativistic
597 electron populations: Ground-based and Van Allen Probes observations, *Geophysical Research Letters*,
598 41, 1375–1381, doi:10.1002/2013GL059024.
599

600 Zhao, H., Baker, D. N., Li, X., Malaspina, D. M., Jaynes, A. N., & Kanekal, S. G. (2019). On the
601 acceleration mechanism of ultrarelativistic electrons in the center of the outer radiation belt: A
602 statistical study. *Journal of Geophysical Research: Space Physics*, 124,
603 <https://doi.org/10.1029/2019JA027111>
604

605 Zong, Q.-G., X.-Z. Zhou, Y. F. Wang, X. Li, P. Song, D. N. Baker, T. A. Fritz, P. W. Daly, M. Dunlop, and A.
606 Pedersen (2009), Energetic electron response to ULF waves induced by interplanetary shocks in the
607 outer radiation belt, *Journal of Geophysical Research*, 114, A10204, doi:10.1029/2009JA014393.

608

609 Zong, Q. R. Rankin, X. Zhou (2017), The interaction of ultra-low-frequency pc3-5 waves with charged
610 particles in Earth's magnetosphere. *Reviews of Modern Plasma Physics*, 1(1), 10, doi: 10.1007/s41614-
611 017-0011-4

612

613

614 Figure Captions

615 Figure 1. Mean daily electron fluxes at 4 energy ranges (>0.23 , >0.6 , >1.5 , and >2.9 MeV) over L=2-9
616 (northern hemisphere).

617 Figure 2. Mean daily lower band chorus PSD over L=2-6 (northern hemisphere).

618 Figure 3. Mean daily ULF power (Pc3, Pc4, and Pc5) at McMAC stations BENN (L=2.5), GLYN (L=3.4), and
619 CARISMA stations PINA (L=4.06), ISLL (L=5.15), GILL (L=6.15), and FCHU (L=7.44).

620

621 Figure 4. Scatterplots of mean daily lower band chorus \log_{10} PSD on previous day (Lag 1) vs. daily change
622 in >1.5 MeV \log_{10} electron flux channel over L=2-6 (a-e). The correlation coefficient (r) is given for each L.

623 Figure 5. Partial correlations between mean daily lower band chorus \log_{10} PSD lagged over 0-3 days and
624 daily change in 4 electron \log_{10} flux energy ranges (>0.23 , >0.6 , >1.5 , and >2.9 MeV) over L=2-7 (a-f)
625 (northern hemisphere). Correlations <0.10 lie within the gray area.

626 Figure 6. Scatterplots of ULF power (Lag 1) and >1.5 MeV electron flux at L=5. a. ULF Pc3, b. ULF Pc4, c.
627 ULF Pc5. All ULF bands show nearly identical correlations with flux.

628 Figure 7. Partial correlations at L=5 between mean daily ULF a. Pc3, b. Pc4, and c. Pc5 over 0-3 days
629 previous and daily change in 4 electron \log_{10} flux energy ranges (>0.23 , >0.6 , >1.5 , and >2.9 MeV).

630 Figure 8. Scatterplots of mean daily ULF Pc5 \log_{10} power on previous day (Lag 1) vs. daily change in >1.5
631 MeV \log_{10} electron flux channel over L=2-7 (a-f). The correlation coefficient (r) is given for each L.

632 Figure 9. Partial correlations between mean daily ULF Pc5 lagged over 0-3 days and daily change in 4
633 electron \log_{10} flux energy ranges (>0.23 , >0.6 , >1.5 , and >2.9 MeV) over L=2-7 (a-f). Correlations <0.10 lie
634 within the gray area.

635 Figure 10. Standardized regression coefficients for each of L=3-6 predicting daily change in 4 electron
636 flux energy ranges (a. >0.23 , b. >0.6 , c. >1.5 , and d. >2.9 MeV) using lower band chorus PSD and ULF Pc5
637 power averaged over the same day (Lag 0; white), the previous day (Lag 1; light blue), and 2 days
638 previous (Lag 2; dark blue) (northern hemisphere). Red lines denote statistically significant coefficients.
639 Percent of variation in flux difference explained by the model is given at the top of each panel. This
640 corresponds to the correlation (r) given within the panel. Lag 1 electron flux is added to each analysis to
641 correct for serial autocorrelation. ULF at GLYN for L=3, PINA at L=4, ISLL at L=5, and GILL at L=6.

642 Figure 11. Predicting change in daily flux using linear and quadratic terms of Lag 0 \log_{10} (ULF Pc5 power)
643 and chorus \log_{10} (PSD) as well as their multiplicative interaction term over L=3-6 (a-d) at 4 flux energy

644 ranges (>0.23 , >0.6 , >1.5 , and >2.9 MeV). Lag 1 electron flux is added to each analysis to correct for
645 serial autocorrelation. ULF at GLYN for L=3, PINA at L=4, ISLL at L=5, and GILL at L=6.

646 Figure 12. Predicting change in daily flux using linear and quadratic terms of Lag 1 \log_{10} (ULF Pc5 power)
647 and chorus \log_{10} (PSD) as well as their multiplicative interaction term over L=4-6 (a-d) at 4 flux energy
648 ranges (>0.23 , >0.6 , >1.5 , and >2.9 MeV). Black arrows indicate examples of strong multiplicative
649 interaction; blue arrows are examples of ULF effect becoming negative at high ULF power when the ULF-
650 VLF multiplicative interaction is strong; green arrows indicate nonlinear increased effect at high ULF
651 power. Lag 1 electron flux is added to each analysis to correct for serial autocorrelation. ULF at GLYN for
652 L=3, PINA at L=4, ISLL at L=5, and GILL at L=6.

Figure 1.

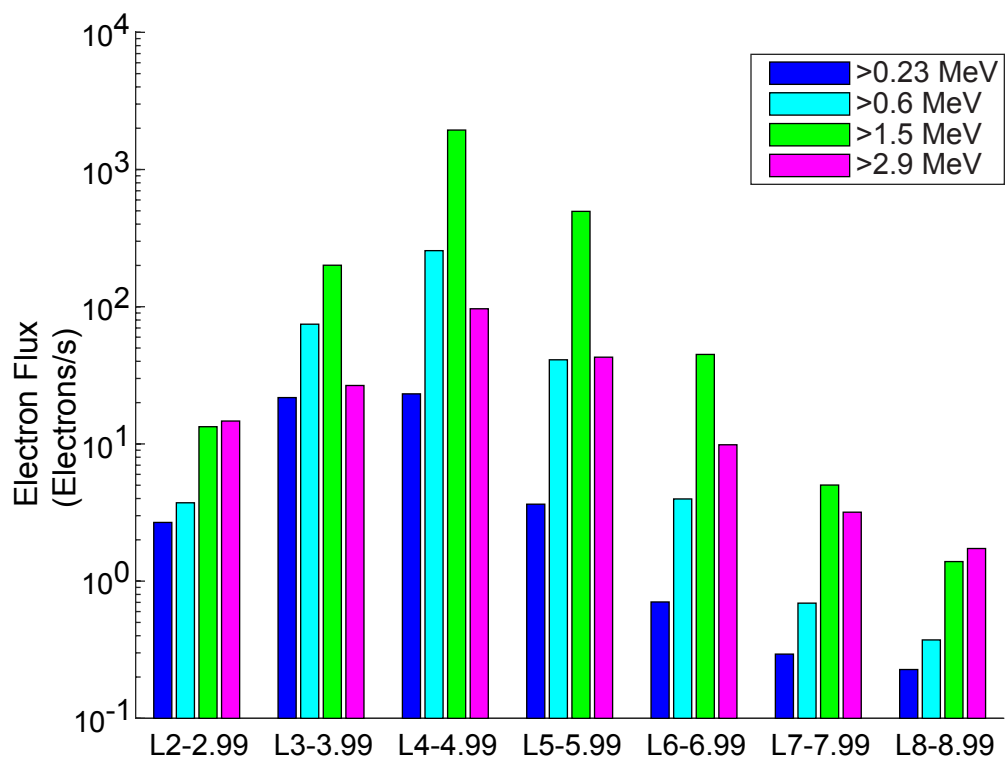


Figure 2.

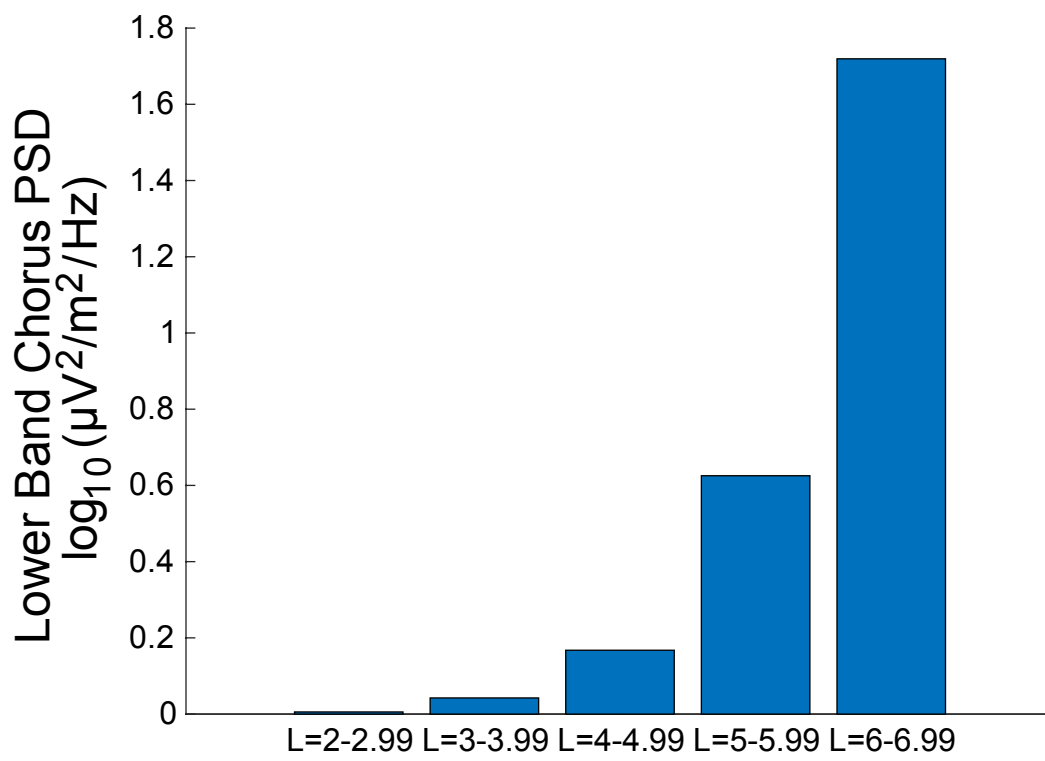


Figure 3.

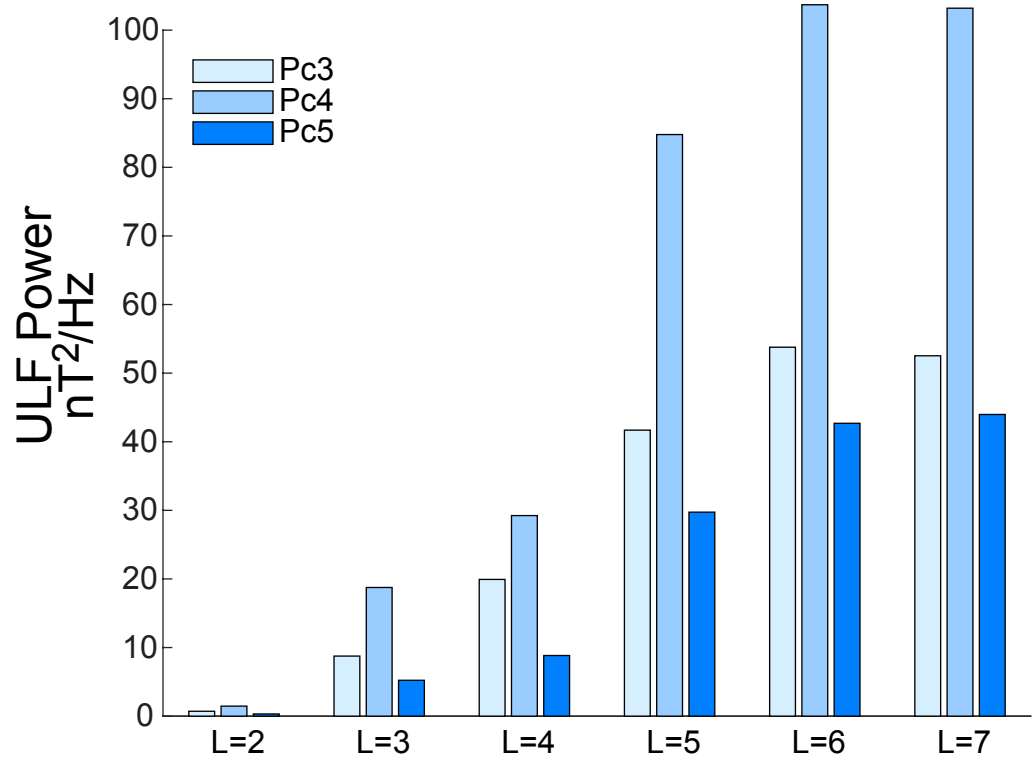


Figure 4.

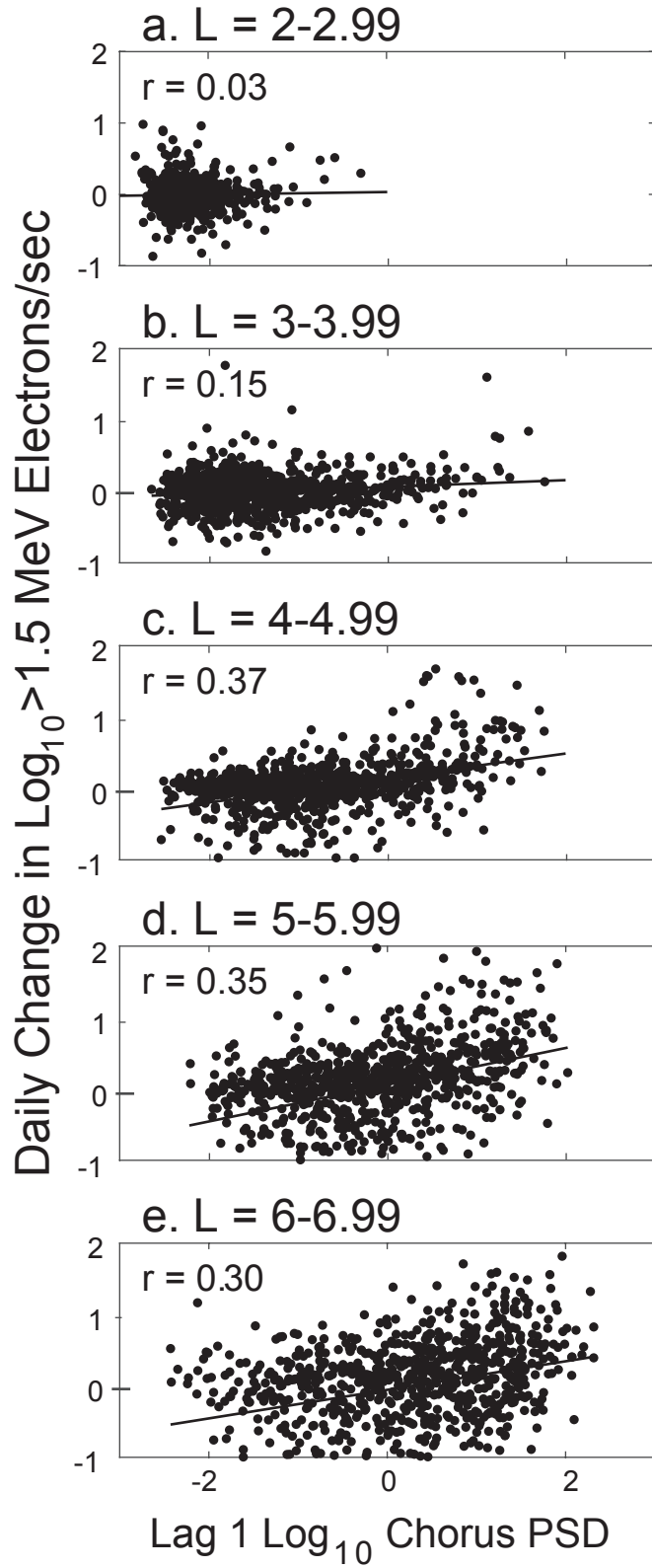


Figure 5.

Partial Correlations of Lower Band Chorus PSD
with Daily Change in Electrons/sec

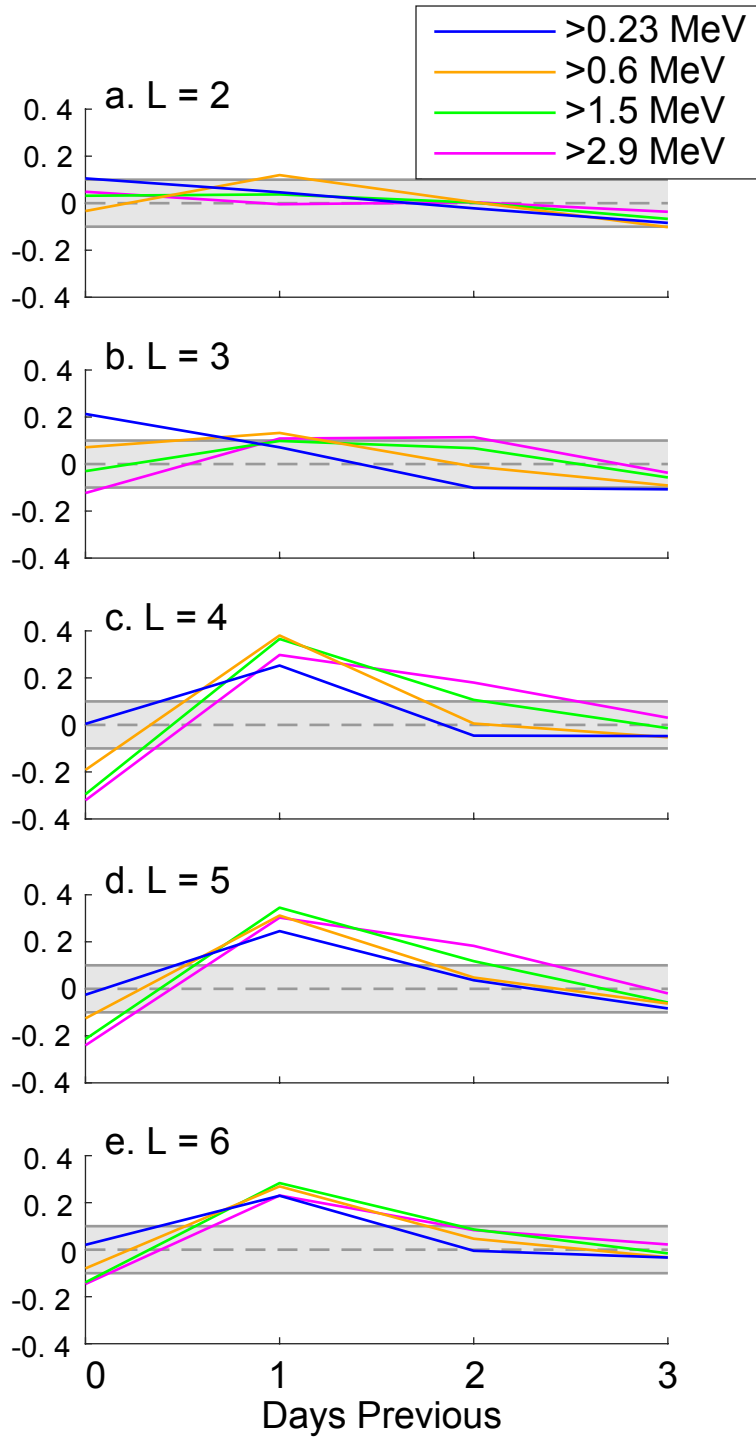
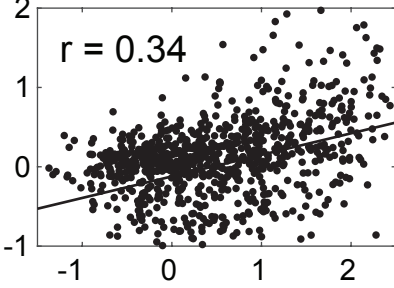


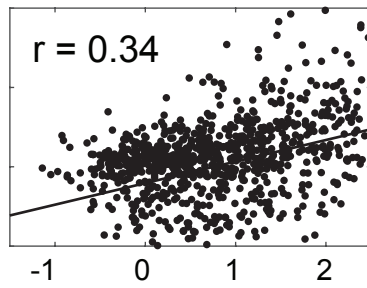
Figure 6.

Daily Change Log_{10}
>1.5 MeV Electrons/sec

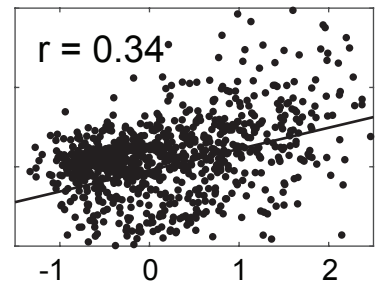
a. ULF Pc3 (L=5)



b. ULF Pc4 (L=5)



c. ULF Pc5 (L=5)



Lag 1 Log_{10} ULF Power

Figure 7.

Partial Correlation of ULF Power (L=5)
with Daily Change in Electrons/sec

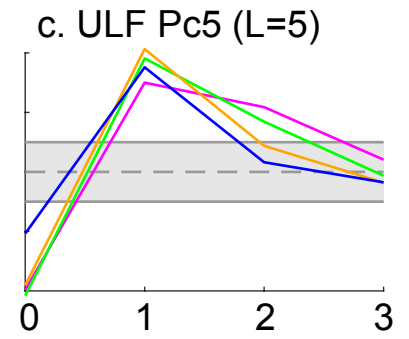
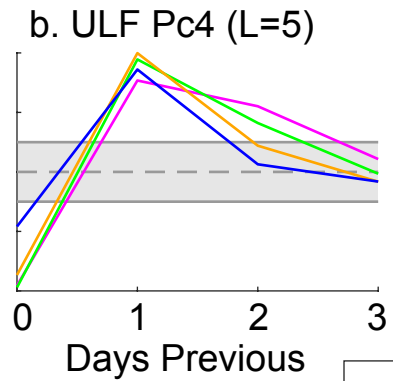
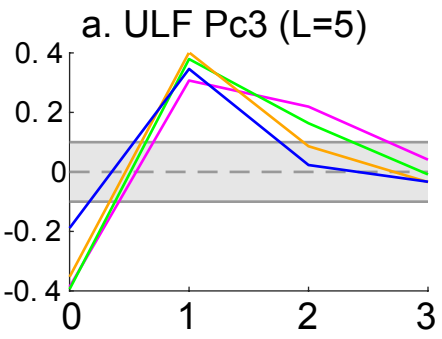


Figure 8.

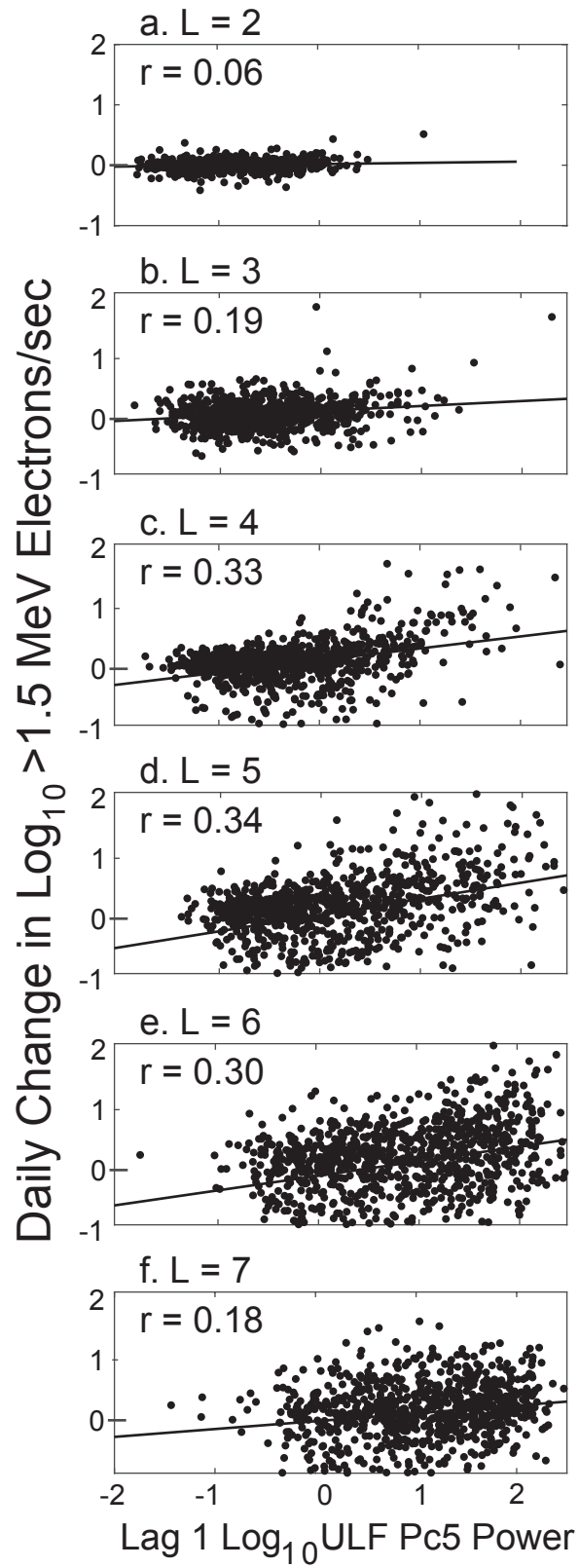


Figure 9.

Partial Correlations of ULF Pc5 Power
with Daily Change in Electrons/sec

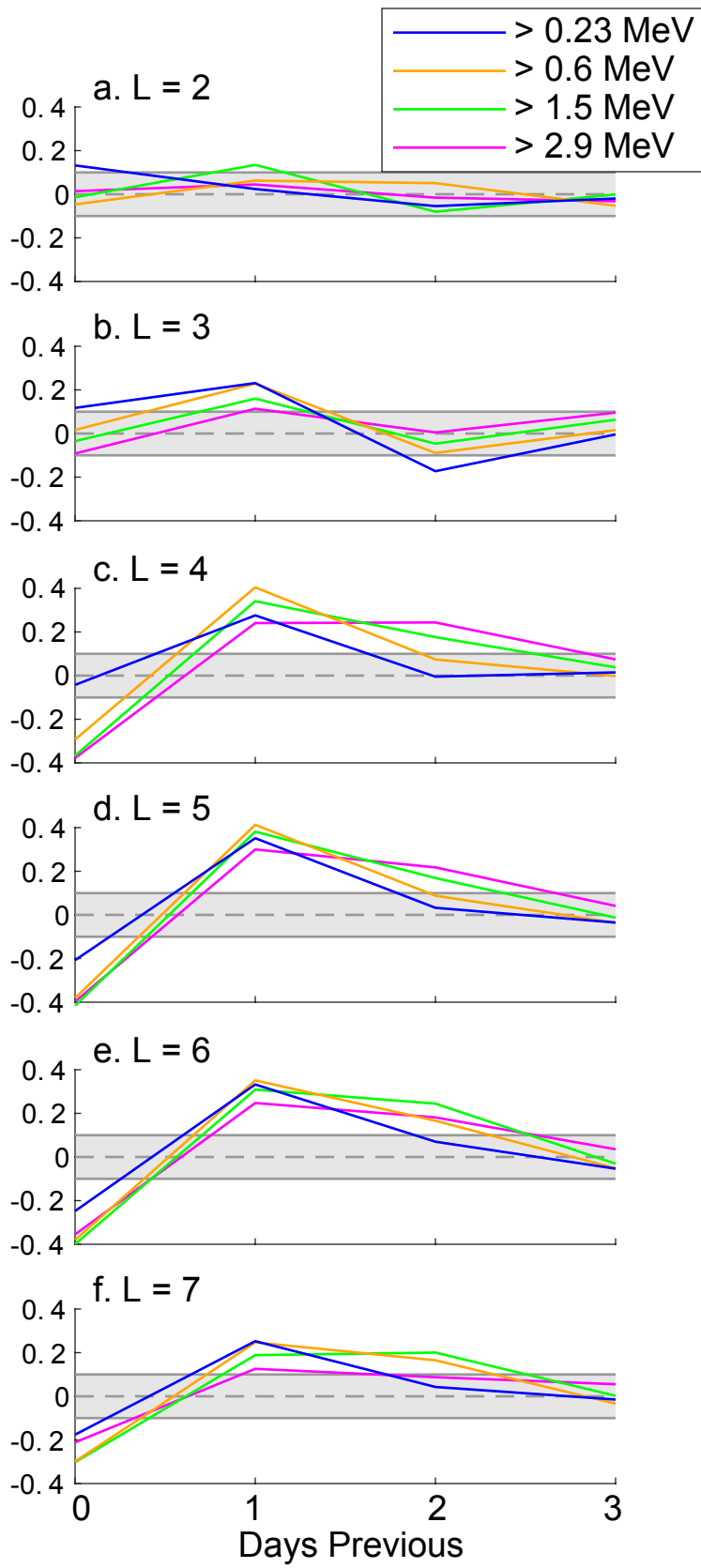


Figure 10.

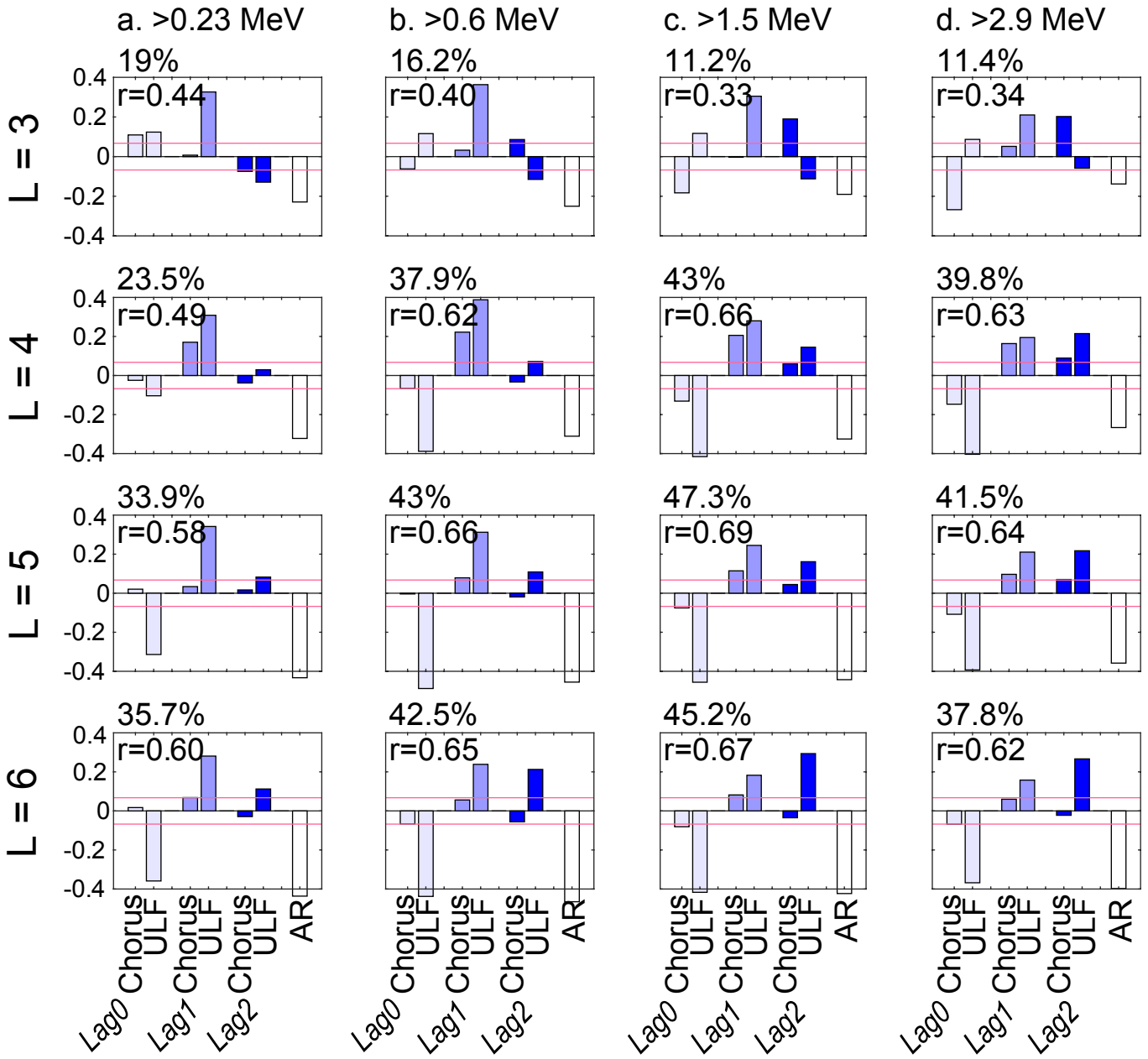


Figure 11.

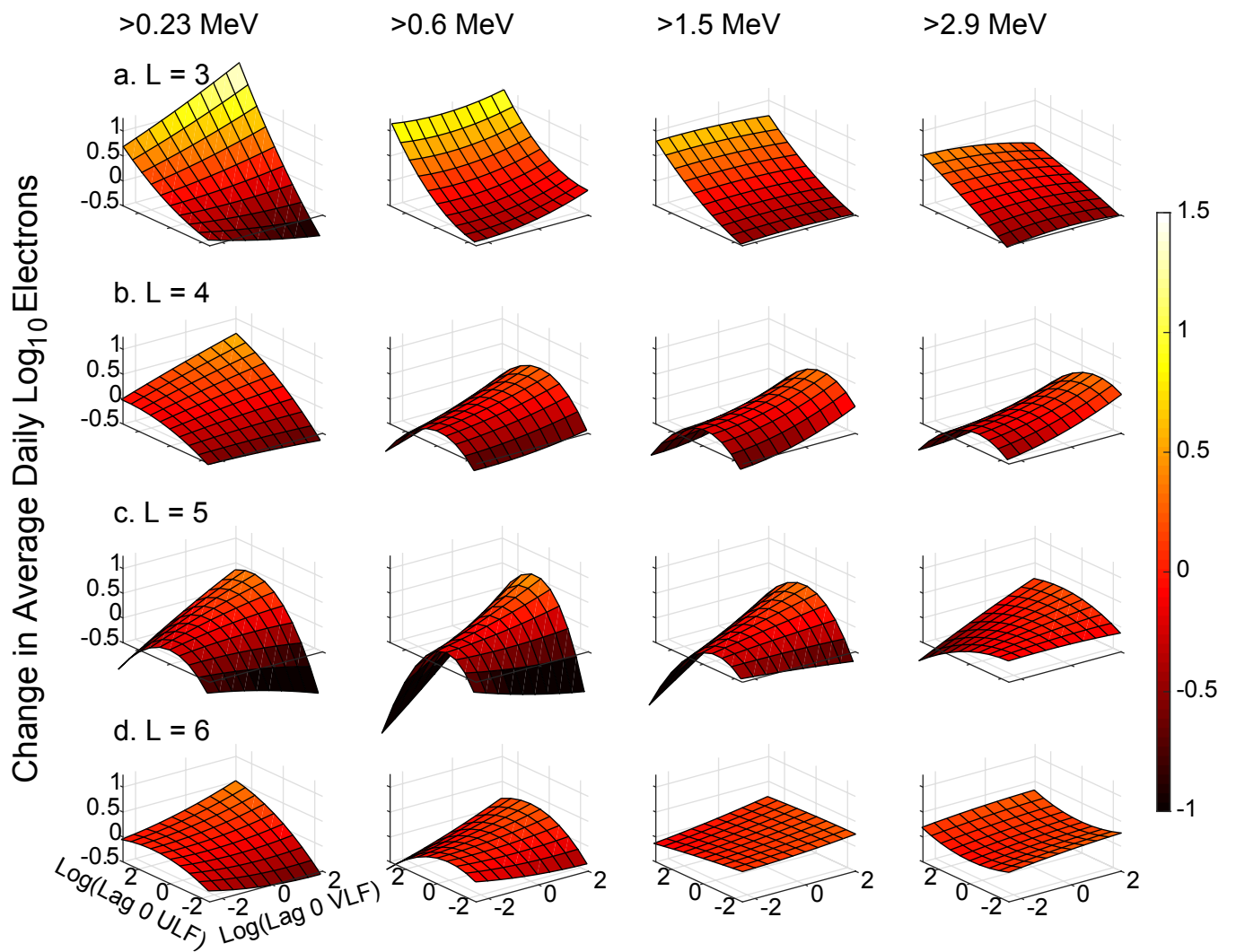


Figure 12.

